ISSN 1028-334X, Doklady Earth Sciences, 2007, Vol. 417, No. 8, pp. 1287–1292. © Pleiades Publishing, Ltd., 2007.
Original Russian Text © I.Yu. Koulakov, 2007, published in Doklady Akademii Nauk, 2007, Vol. 417, No. 2, pp. 251–257.

GEOPHYSICS

Structure of the Afar and Tanzania Plumes Based on the Regional Tomography Using ISC Data

I. Yu. Koulakov

Presented by Academician N.L. Dobretsov January 12, 2007

Received February 6, 2007

DOI: 10.1134/S1028334X07080363

Establishment of the correlation between deep dynamics and processes observed at the daytime surface is an important fundamental problem of modern geodynamics. The study of mantle plumes, which are responsible for volcanic processes and riftogenesis in different parts of the Earth, occupies a special place in this problem. The system of rift depressions in East Africa and the Afar triple junction is the most striking example of the influence of mantle processes on the near-surface tectonic activity. The correlation between mantle dynamics and riftogenesis in this region has attracted the attention of many scholars around the world (see, for example, [1]). Quantitative estimates of pull-apart forces in the lithosphere induced by an ascending plume are estimated in [2]. These works and a multitude of other observations demonstrate that rifting in East Africa is caused precisely by mantle processes.

The Afar triple junction (ATJ) is a transition case from continental rifting to oceanic spreading (Fig. 1). Three branches of divergence of the lithosphere located at almost equal angles (120°) with respect to each other are observed around the ATJ. Two branches (the Red Sea and the Gulf of Aden) are incipient oceans with prominent spreading zones. The third branch (the Ethiopian Rift) is the beginning of a large system of depressions extended along the African continent first to the southwest and then to the south. The total length of the East African Rift is more than 2500 km.

At a distance of approximately 700 km from the ATJ, the rifting is attenuated and then resumes again along two branches around the Tanzania Craton (Western and Eastern rifts). The Eastern Rift is also called the Kenya Rift in the literature, while the Western Rift is called Tanganyika Rift (from the name of Lake Tanganyika). The riftogenesis along the entire length of the East African Rift is accompanied by active volcanic processes (see, for example, [3]).

The East African Rift can be divided into two approximately equal (Ethiopian and Tanzanian) segments by the topography and volcanic activity (Fig. 1). Regional rises in these two segments 1000–1500 m high can evidence that the mantle beneath them is characterized by significant deconsolidation, which promotes the ascent of matter. Usually, these phenomena are associated with one or two plumes. This is also confirmed by the analysis of the composition of volcanic rocks along the rifts, which point to a significant deep component of the magmas [4]. The problem whether the Ethiopia and Tanzania rift systems are independent or whether they are controlled by one mantle plume is still open. The geochemical data do not give unambiguous solution to this problem. For example, the authors of [3] state that all volcanoes of the East African Rift are fed from one plume. On the other hand, the authors of [5] speak about two independent plumes.

The Afar Plume is clearly seen in all global tomographic models in the upper mantle [6]. However, the limited resolution does not allow us to distinguish its detailed structure in these models. On the other hand, several experiments were carried out to deploy temporal seismological networks for conducting teleseismic inversion based on the runtime of beams from remote events [7–10]. However, due to political problems, deployments of the stations were local and only fragmentary data were obtained about individual parts of the plume as a result of these investigations.

The authors of [11, 12] presented the inverse tomographic scheme (ITS), which is based on the runtimes of signals from earthquakes located in the study region and recorded on the global seismological network stations. In the current work, we describe the results of applying the ITS in the Afar Plume and East African Rift region, which allowed us to obtain more detailed structures of the upper mantle than in the global models. At the same time, these structures are more integrated than in local teleseismic models.

Institute of Geology and Mineralogy, Siberian Division, Russian Academy of Sciences, pr. akademika Koptyuga 3, Novosibirsk, 630090 Russia; e-mail: kul@uiggm.nsc.ru

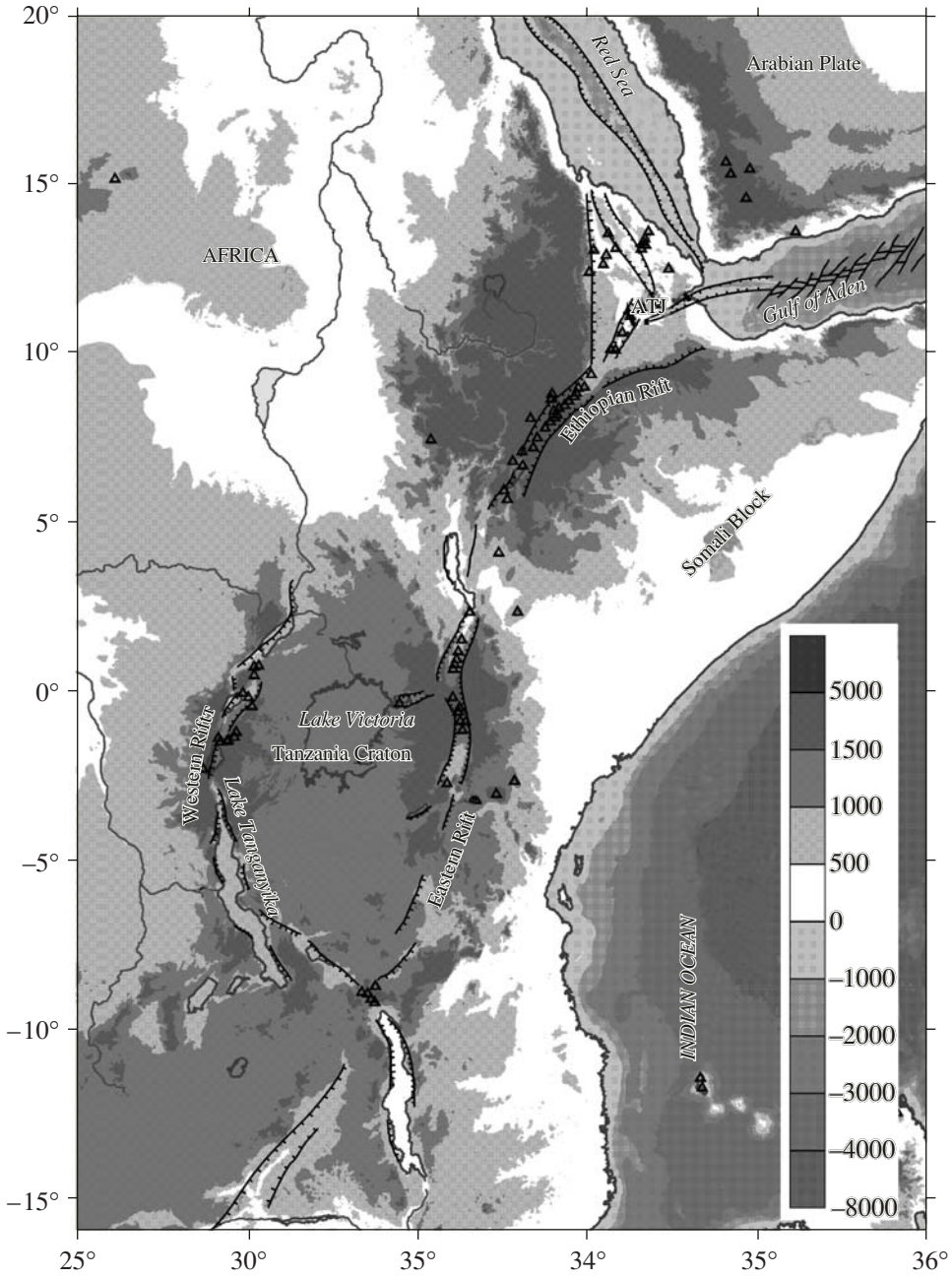

Fig. 1. The location of the East African rift system and surrounding territories. Topography and bathymetry are given in meters. Lines with ticks show the edges of the rift troughs. Triangles denote active volcanoes with an age not older than 2 Ma. (ATJ) Afar triple junction.

DESCRIPTION OF THE DATA AND ALGORITHM

In this study, we used the data of the International Seismological Center (ISC) during the period from 1964 to 2001, which contains information about arrival times of signals from earthquakes at more than 7000 stations of the global seismological network. The authors of [11, 12] showed that the ITS allows us to obtain stable structures even in regions without seismic stations. It should be noted that the presence of stations within the study region increases significantly the stability of the solution because this allows us to localize the events better. Similarly to previous works, inversion was performed in several mutually overlapping circular regions, which were later united in one model. We used a total of five circles located along the axis of the East African Rift. The radius of four circles was 8°, while the radius of the fifth circle with the center in the Afar junction was equal to 9°. The inversion over fragments is carried out because the optimal operation of the ITS

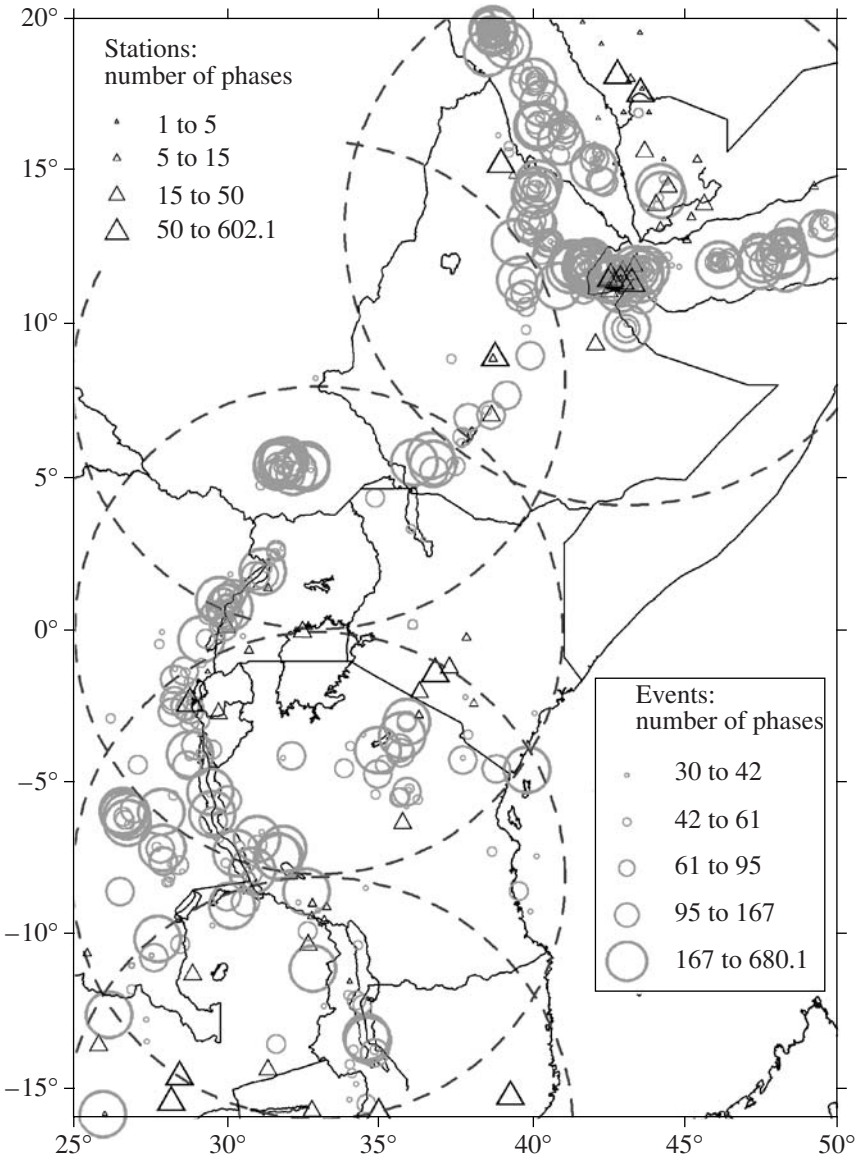

Fig. 2. Configuration of the observation system in this work. Dashed circles denote the location of five regions for which independent calculations were performed. Gray circles denote earthquakes. Triangles denote recording stations. The sizes of the circles and triangles reflect the number of phases corresponding to the sources and receivers used in the work.

is provided when the lateral size of the study region is approximately two times greater than the vertical size.

We selected a total of 583 sources located in these circular regions (Fig. 2). During their selection, the minimal number of phases was equal to 30 and the minimal empty azimuthal segment did not exceed 180°. In the calculations of the theoretical runtimes, we took into account the Earth's ellipticity, the variable Moho thickness in accordance with the global model, and the elevation of stations above sea level. A total of ~67 000 P-phases and 6147 S-phases remained as a result of quality evaluation after localizing the sources. A number of S-phases more than 10 times smaller (as compared to the P-phases) leads to a significantly lower level of the S-model resolution, which will be shown in the synthetic tests.

The details of the inversion algorithm are described in more detail in [11]. According to this tomographic scheme, the distribution of anomalies of P- and S-seismic velocities is calculated at the nodes of a grid, which are located at horizontal levels at depths ranging from 50 to 670 km according to the density of beams. The inversion is performed simultaneously for the distribution of P- and S-velocity anomalies and parameters of the sources (coordinates and time in the source).

RESULTS AND TESTING

The results of inversion for models of P- and S-velocities are shown in the left column of Fig. 3. The most prominent anomaly is observed in the region of the Afar triple junction in both P- and S-anomalies at all

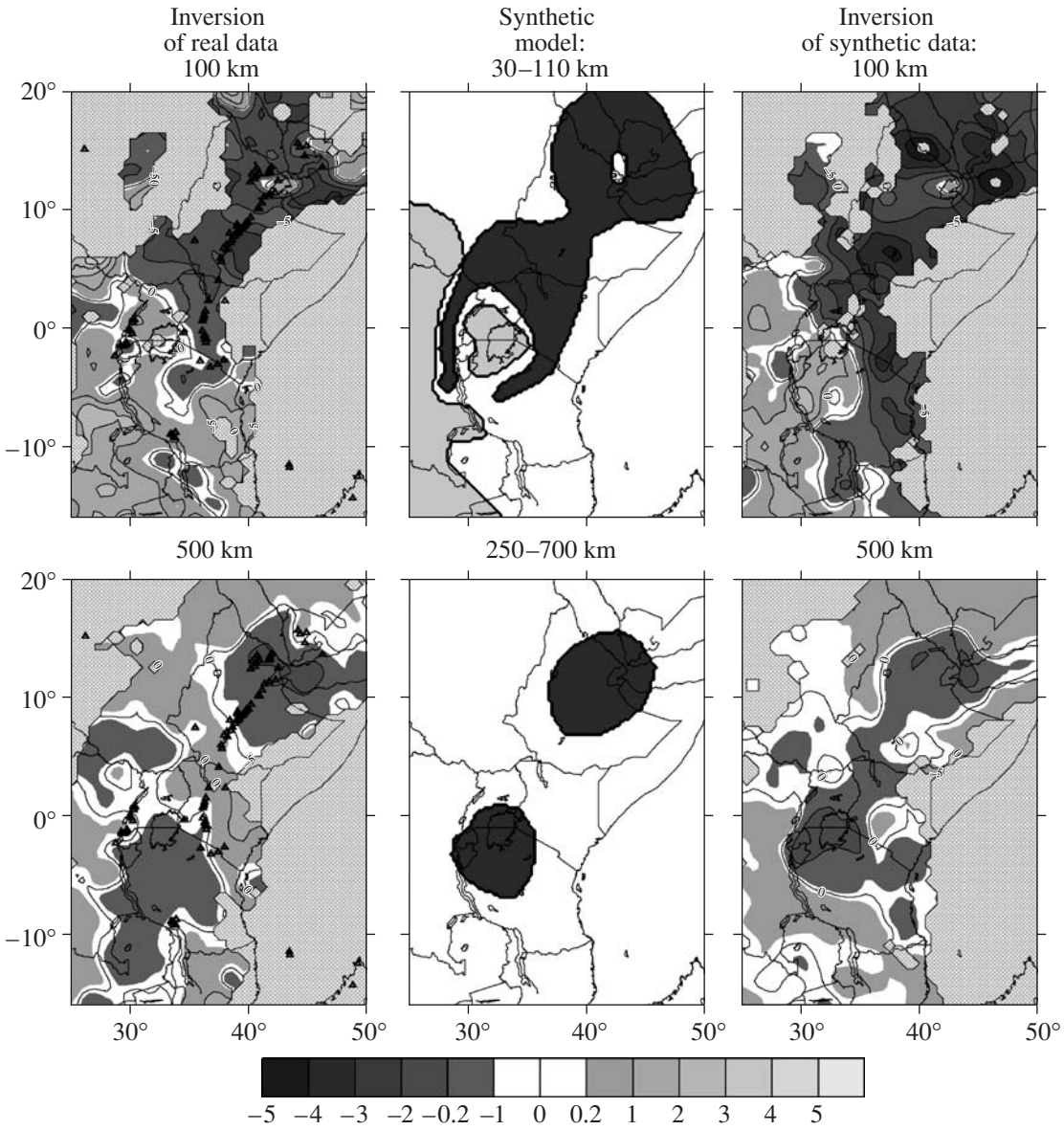

Fig. 3. Results of inversion of real data and restored configuration of anomalies by means of synthetic modeling. An example is shown for the P-model at depths of 100 and 500 km.

depth intervals. At greater depths, this anomaly is seen as an isometric body with a size of 600–800 km, while it spreads over a significantly larger territory at smaller depths. It should be noted that the amplitude of the anomaly is 2–3 times weaker at greater depths than at higher sections. However, this hardly reflects the real relations as will be shown below using synthetic modeling. The lower amplitude at lower sections can be related to lesser density of beams.

It should be noted that a smaller high-velocity anomaly can be seen within the dominating low-velocity anomaly in the region of the Afar triple junction. A similar structure is also observed in the regions of other plumes in the spreading zones.

The reliability of this and other distinguished anomalies was studied in a series of synthetic tests. The essence of the tests is in specifying an artificial structure of seismic inhomogeneities (a chessboard or actually expected anomalies) and calculation of runtimes in this model based on the beams used in the real system of observations. Next, noise with a level close to that expected in the real data (with dispersion of 0.2 and 0.5 s for the P-and S-data) is added to the synthetic runtimes. After calculating the synthetic runtimes, we complete the inversion procedure (including the absolute localization of the sources) regions. All free parameters for the inversion were selected the same as in the case of processing real data.

Here, we present the results of only one test, whose objective is in contriving a model that restores the configuration of the anomalies after inversion similar to the real data observed after inversion. The initial synthetic anomalies were specified in the form of prisms in three layers: 30–110 km, 110–250 km, and 250–700 km. Their configurations are shown in the middle column of Fig. 3.

The upper layer reflects the lithosphere structure. Large thick African and Tanzania cratons are presented by an elevated anomaly (+3%). The head of the Afar Plume, which merges with the Kenya Plume, is represented by an anomaly with lower velocities (–4%). A relatively small hole with zero amplitude is specified for the P-model within the Afar Plume. In the S-model, this anomaly remains negative with greater amplitude than the background value (–5%). In the second layer modeling the asthenosphere, the model is a high-velocity root of the African Craton (+3%) and merged heads of the Afar and Kenya plumes (–4%). In the deeper layer, two separate plumes of the same shape and amplitude (–4%) are modeled. The shape and amplitude of the anomalies presented in this model were obtained as a result of many attempts, which resulted in gaining the maximal similarity between the results of inversion of the real and synthetic data. The right column in Fig. 3 shows the results of restoration. One can see that all main anomalies are restored correctly, and the results of the synthetic inversion are similar to the results of processing the real data shown in the left column of Fig. 3.

It is worth noting that the amplitude of the restored anomalies is much lower than the values in the initial model. The decrease is particularly significant at great depths. This example points to the problem of ambiguity in determination of the amplitude of anomalies, which is typical for all types of tomographic inversions. At the same time, it is possible to estimate the real value of an anomaly based on the results of this test. For example, if anomaly –4% at a depth of 400–500 m is seen as anomaly –1% in the synthetic reconstruction, it is possible to say that the inverse statement is also correct. In other words, if we have 1% as a result of inversion of the real data, the amplitude of the anomaly is 4% in the real Earth.

In addition to this test, we also carried out the chessboard test, which demonstrated a reliable reconstruction of anomalies with a size of 400 km in the P-model and 600 km in the S-model.

DISCUSSION

Inversion of the ISC data yielded the upper mantle pattern of inhomogeneities beneath the Afar triple junction and East African Rift. The reliability of the obtained images was demonstrated by means of synthetic testing. A model for interpretation of the obtained results was contrived (Fig. 4). We suppose that the dynamics of the East African Rift is determined by the existence of two plumes: Afar and Tanzania. There are no grounds to think that these plumes differ principally in power or size at large depths. In both cases, the size of these anomalies at a depth of 500 km is approximately 600 km. It is likely that this value shows the size of the region heated by the plumes rather than the size of the plumes. The authors of [13] showed that powerful plumes (~100 km in diameter), such as the Afar and Tanzania plumes, can cause warming and chemical alterations in a region of ~200 km around the plumes, which approximately corresponds to the size of the observed anomalies. Another piece of evidence for the existence of two separate plumes beneath the East African Rift can be seen in the topography of the study region (Fig. 1). One can clearly see two isometric domes with similar sizes and amplitudes.

Despite the fact that the Tanzania and Afar plumes possibly have similar characteristics in the depths, their influence on surficial processes appears to be principally different. According to our model, the Afar Plume reaches the base of the relatively thin lithosphere and divides it into three segments at an angle of 120°. This leads to the formation of two spreading zones (in the Red Sea and the Gulf of Aden) and the Ethiopian rift system. Judging from our data and other geophysical data, the Tanzania Plume is rising exactly beneath the Tanzania Craton, where the lithosphere is expected to be quite thick. The plume cannot divide this lithosphere (as at the Afar triple junction) and spreads along its base. An already weakened plume flows reach the edge of the craton. Nevertheless, their intensity appears sufficient for the opening of the western and eastern branches of the East African Rift.

Is this a mere coincidence that the head of the plume appeared beneath the thick lithosphere of the craton? The results of numerical modeling [14] demonstrate that this situation is quite natural. The thick lithosphere of the cratons attracts ascending flows in the mantle and initiates the formation of plumes. This means that similar processes can also occur beneath other cratons, for example, the Siberian Craton.

An interesting feature is observed within the Afar Plume in the form of a local high-velocity anomaly. Three alternative hypotheses can be suggested to explain this anomaly. According to the first hypothesis, high velocities at the axis of the plume are explained by anisotropy. The beams, which predominantly propagate along the vertical direction in our observation system, appear faster in the area of maximal velocity of matter ascent in the plume due to the dominating vertical orientation of olivine crystals in the plume. According to the second hypothesis, high velocities in the plume are caused by the ascent of abyssal matter, which has a different (higher velocity) composition. The third hypothesis is based on the supposition about the existence of a reverse descending current in the plume put forward by N.L. Dobretsov and A.G. Kirdyashkin in [13, 15].

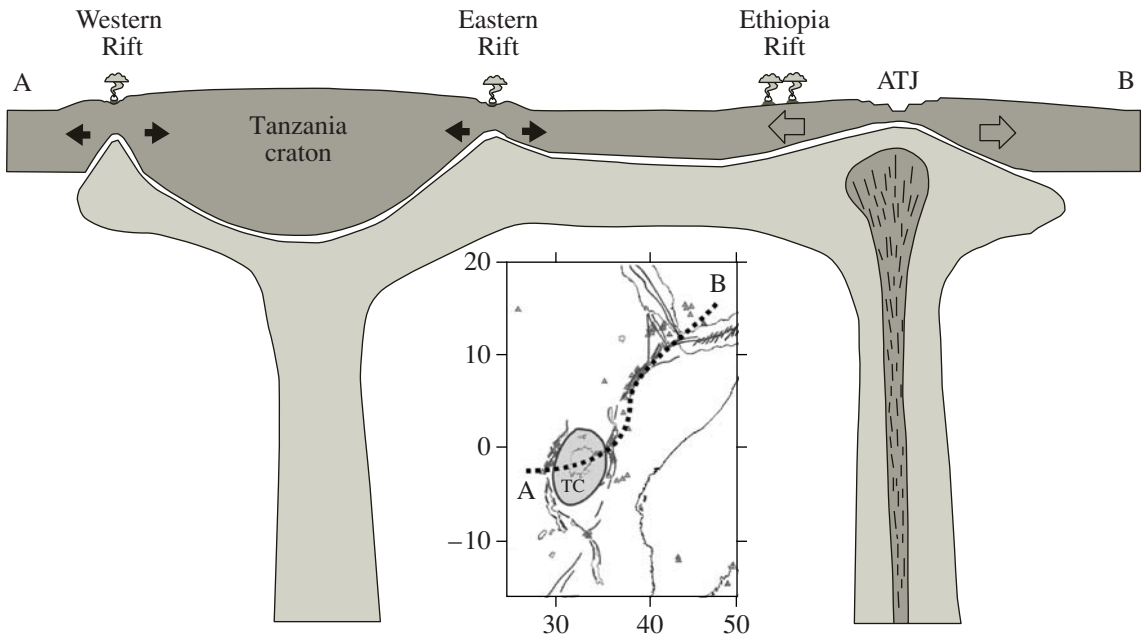

Fig. 4. Scheme for interpretation of the structure under the East African Rift. The inset shows a chart of the region with the approximate location of the profile (heavy dashed line), for which the scheme is shown. (ATJ) Afar triple junction; (TC) Tanzania Craton.

Thus, based on physical modeling, we demonstrated the possibility of descending motions of colder matter in the ascending plume center. It is possible that precisely this process is observed in the obtained tomographic images.

REFERENCES

1. N. Logatchev, Y. Zorin, and V. Rogozhina, Tectonophysics **94**, 223 (1983).
2. R. Westaway, Earth Planet. Sci. Lett. **119**, 331 (1993).
3. C. Ebinger and N. Sleep, Nature **395**, 788 (1998).
4. J.-M. Kendall, G. Stuart, N. Ebinger, et al., Nature **433**, 146 (2005).
5. R. George, N. Rogers, and S. Kelley, Geology **26**, 923 (1998).
6. H. Bijwaard, W. Spakman, and E.R. Engdahl, J. Geophys. Res. **103**, 30055 (1998)
7. U. Achauer and the KRISP Teleseismic Working Group, Tectonophysics **236**, 305 (1994).
8. I. D. Bastow, G. W. Stuart, J.-M. Kendall, et al., Geophys. J. Int. **162**, 479 (2005).
9. A. A. Nyblade and C. A. Langston, EOS Trans. AGU **83**, 405 (2002).
10. J. Ritsema, A. Nyblade, T. J. Owens, et al., J. Geophys. Res. **103**, 21201 (1998).
11. I. Koulakov and S. V. Sobolev, Geophys. J. Int. **164**, 425 (2006).
12. I. Koulakov, S. A. Tychkov, N. A. Bushenkova, et al., Tectonophysics **358**, 77 (2002).
13. N. L. Dobretsov, A. G. Kirdyashkin, and A. A. Kirdyashkin, *Deep Geodynamics* (SO RAN, Filial Geo, 2001) [in Russian].
14. S. A. Tychkov, A. N. Vasilevskii, and E. V. Rychkova, Geol. Geophys. **40**, 1182 (1999).
15. N. L. Dobretsov, A. A. Kirdyashkin, A. G. Kirdyashkin, et al., Petrology **14**, 477 (2006) [Petrologiya, **14**, 508 (2006)].